Intensification of premonsoon tropical cyclones in the Bay of Bengal and its impacts on Myanmar

Shih-Yu Wang,[1,2] Brendan M. Buckley,[3] Jin-Ho Yoon,[4] and Boniface Fosu[2]

Received 21 November 2012; revised 8 March 2013; accepted 5 April 2013.

[1] We analyze multiple global reanalysis and precipitation datasets in order to explain the dynamic mechanisms that lead to an observed intensification of the monsoon trough and associated tropical cyclone (TC) activity over the Bay of Bengal (BOB) during the premonsoon month of May. We find that post-1979 increases in both premonsoon precipitation and TC intensity are a result of enhanced large-scale monsoon circulation, characterized by lower-level cyclonic and upper-level anticyclonic anomalies. Such circulation anomalies are manifest of the tropospheric expansion that is caused by regional warming. The deepened monsoon trough in the BOB not only affects TC frequency and timing, but also acts to direct more cyclones towards Myanmar. We propose that increasing sea surface temperature in the BOB has contributed to an increase in cyclone intensity. Our analyses of the Community Earth System Model single-forcing experiments suggest that tropospheric warming and a deepening of the monsoon trough can be explained by two discreet anthropogenic causes—an increase in absorption due to aerosol loading and an increase in the land-ocean thermal contrast that results from increased greenhouse gases. The ensuing circulation changes provide favorable conditions for TCs to grow and to track eastward towards Myanmar.

Citation: Wang, S.-Y., B. M. Buckley, J.-H. Yoon, and B. Fosu (2013), Intensification of premonsoon tropical cyclones in the Bay of Bengal and its impacts on Myanmar, *J. Geophys. Res. Atmos.*, *118*, doi:10.1002/jgrd.50396.

1. Introduction

[2] The monsoon trough over South Asia first develops in May over the Bay of Bengal (BOB), as seen in Figure 1a by the 850-mb streamfunction (SF), and its development leads to a stark contrast in monsoon onset between the two shores of the BOB [*Krishnamurti et al*., 1981; *Wu et al*., 2012]. While the monsoon onset in eastern India starts in early June, the onset in Myanmar occurs almost a month earlier at the beginning of May [*Fasullo and Webster*, 2003; *Htway and Matsumoto*, 2011]. Together with the seasonal warming of sea surface temperature (SST) that also peaks in May, formation of the BOB monsoon trough also provides favorable conditions for tropical cyclones (TCs). There are two TC seasons in the BOB, one concentrated in May (premonsoon or spring) and the other spanning October-November (postmonsoon or fall). In between the spring and fall seasons, monsoon depressions become active in the BOB, but seldom grow to TC force owing to increased vertical easterly shear during the mature monsoon phase [*Yanase et al*., 2010; *Yokoi and Takayabu*, 2010; *Girishkumar and Ravichandran*, 2012]. Spring TCs mainly develop from low-pressure systems in the equatorial Indian Ocean that then migrate northward into the BOB [*Krishna*, 2009; *Ng and Chan*, 2012]. This is in contrast to fall TCs that often develop from either easterly waves or residual TCs propagating from the Western Pacific under prevailing easterly flows (Figure 1b). As a result, spring TCs feature rather irregular trajectories with wider impacts over Myanmar (Figure 1a).

[3] Since the 1990s, the number of TCs that have made landfall over Myanmar has increased [*Hoarau et al*., 2012]. *Yu and Wang* [2009] predicted that the potential intensity of TCs will increase with rising air temperature [*Yu and Wang*, 2009], a tendency that might be given credibility by the three hurricane-force TCs that struck Myanmar during the almost consecutive years of 2004 (#01 unnamed), 2006 (Mala), and 2008 (Nargis). In particular, Cyclone Nargis caused such severe damage and devastation to Myanmar in May 2008 it was comparable to the 2004 tsunami tragedy in South Asia [*Webster*, 2008]. As we will demonstrate, during the past 30 years, the frequency and intensity of TCs in the BOB in general, and those that directly impacted Myanmar, have increased significantly.

[4] *Singh et al*. [2000] noted an increase in TC number and intensity over the northern Indian Ocean, which they attributed to a decrease in the strength of the tropical easterly jet and a corresponding weakening of the vertical wind shear [*Rao et al*., 2008]. In the neighboring Arabian Sea, *Evan*

[1]Utah Climate Center, Utah State University, Logan, Utah, USA.
[2]Department of Plants, Soils, and Climate, Utah State University, Logan, Utah, USA.
[3]Lamont-Doherty Earth Observatory, Columbia University, Palisades, New York, USA.
[4]Pacific Northwest National Laboratory, Richland, Washington, USA.

Corresponding author: S.-Y. Wang, 4820 Old Main Hill, Logan, UT 84341, USA. (simon.wang@usu.edu)

2169-897X/13/10.1002/jgrd.50396

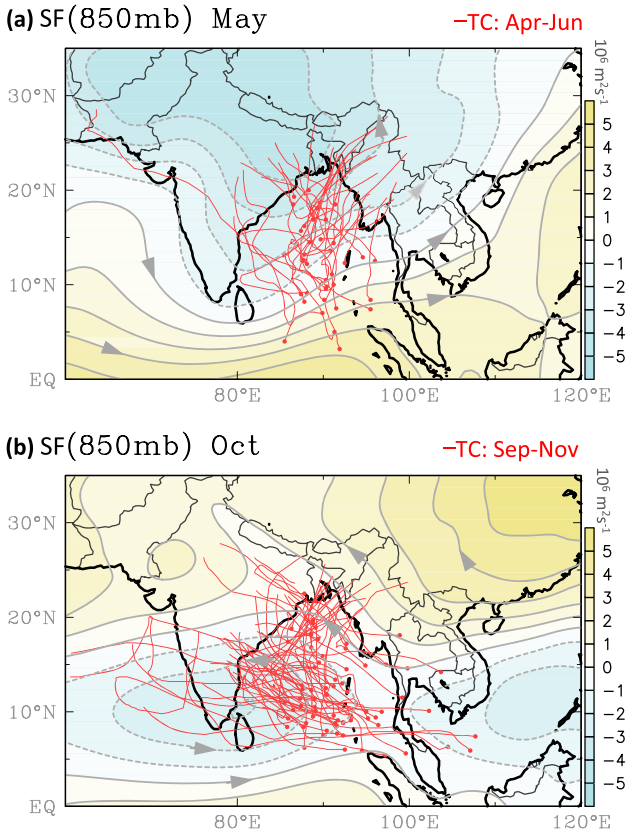

Figure 1. Mean 850-mb streamfunction (SF) of ERA-I for (a) May and (b) October overlaid with 6-h TC tracks in the BOB (red lines) during April-June and September-November, over the period of 1979–2011.

et al. [2011] suggested that the anomalous circulation and reduced vertical shear that led to the intensification of premonsoon TCs is radiatively forced by anthropogenic aerosols. However, the role of reduced vertical shear was questioned by *Wang et al*. [2012], who argued that the dominant factor lies in the increased land-ocean thermal contrast due to aerosols enhancing moisture convergence. Moreover, recent research has found that monsoon onset in the vicinity of the BOB has advanced by 5–10 days since 1979 [*Kajikawa et al*., 2012]. Because winter crops are often stressed prior to the arrival of monsoon rains, any changes in the monsoon onset and spring TC activity, both important rain producers, may become increasingly influential to the premonsoon source of moisture over Myanmar, and hence may be highly significant for agricultural planning.

[5] In this study, we examined the observed changes of spring TC frequency, intensity, and movement over the BOB, along with premonsoon precipitation over Myanmar. We focus on Myanmar because of its high vulnerability to such extreme weather systems, because it has only recently started recovery from decades of civil wars and isolation, and because it lacks adequate capability for disaster response [*Webster*, 2008]. In terms of analysis, we adapted a multiple-data approach that utilizes an array of gridded precipitation and global reanalysis datasets. We employ such an approach because of the uncertainty in the precipitation and assimilation data over steep terrains, especially over Myanmar.

Table 1. Global Reanalysis and Model Datasets Used

Name	Full Name	Agency
MERRA	Modern-Era Retrospective Analysis for Research and Applications	National Aeronautics and Space Administration (NASA)
ERA-Interim	ECMWF Interim Reanalysis Project	European Center for Medium-Range Weather Forecasts (ECMWF)
CFSR	Climate Forecast System Reanalysis	National Oceanic and Atmospheric Administration (NOAA)
ERA-40	ECMWF 40-year Reanalysis Project	ECMWF
CESM	Community Earth System Model (v1)	National Center for Atmospheric Research & Pacific Northwest National Laboratory

These datasets are introduced in section 2, while trends of TC data in the BOB are shown in section 3, the analyses of environmental conditions are presented in section 4, attribution from modeling analysis is given in section 5, and summary and conclusions are provided in section 6.

2. Data Sources

[6] Gridded precipitation datasets provide a complete coverage over most geographical regions around the world. However, previous studies have raised concerns about quality deficiency over data-poor regions, and problems associated with the domain averaging approach for trend analysis [*Ghosh et al*., 2009; *Wang et al*., 2011]. Such concerns are understandably important when conducting analysis for Myanmar and the BOB, where in-situ observations are sparse. In addition, trend analysis using a single reanalysis/gridded dataset has also led to concerns related to changing observation systems that can produce spurious trends [*Paltridge et al*., 2009]. Therefore, in order to obtain a reliable or optimal estimate of any long-term trend, we utilized an array of global reanalysis together with seven gridded precipitation datasets. For the global reanalysis, we used the three most recent datasets that cover the satellite era since 1979: MERRA [*Rienecker et al*., 2011], CFSR [*Saha et al*., 2010], and ERA-Interim [*Simmons et al*., 2007]. The acronym, full name, and description of each are provided in Table 1. For the pre-1979 analysis, we

Table 2. Global Precipitation Datasets Used

Name	Full Name	Spatial Resolution
GPCP	Global Precipitation Climatology Project v2	2.5° long. x lat.
CMAP	Climate Prediction Center Merged Analysis of Precipitation	2.5° long. x lat.
GPCC	Global Precipitation Climatology Center v4	1.0° long. x lat.
UDEL	University of Delaware gauge-based precipitation	0.5° long. x lat.
PREC/L	NOAA's Precipitation Reconstruction over Land	1.0° long. x lat.
CRU	Climate Research Unit	1.0° long. x lat.
APHRODITE	Asian Precipitation - Highly Resolved Observational Data Integration Towards Evaluation	0.5° long. x lat. (daily)

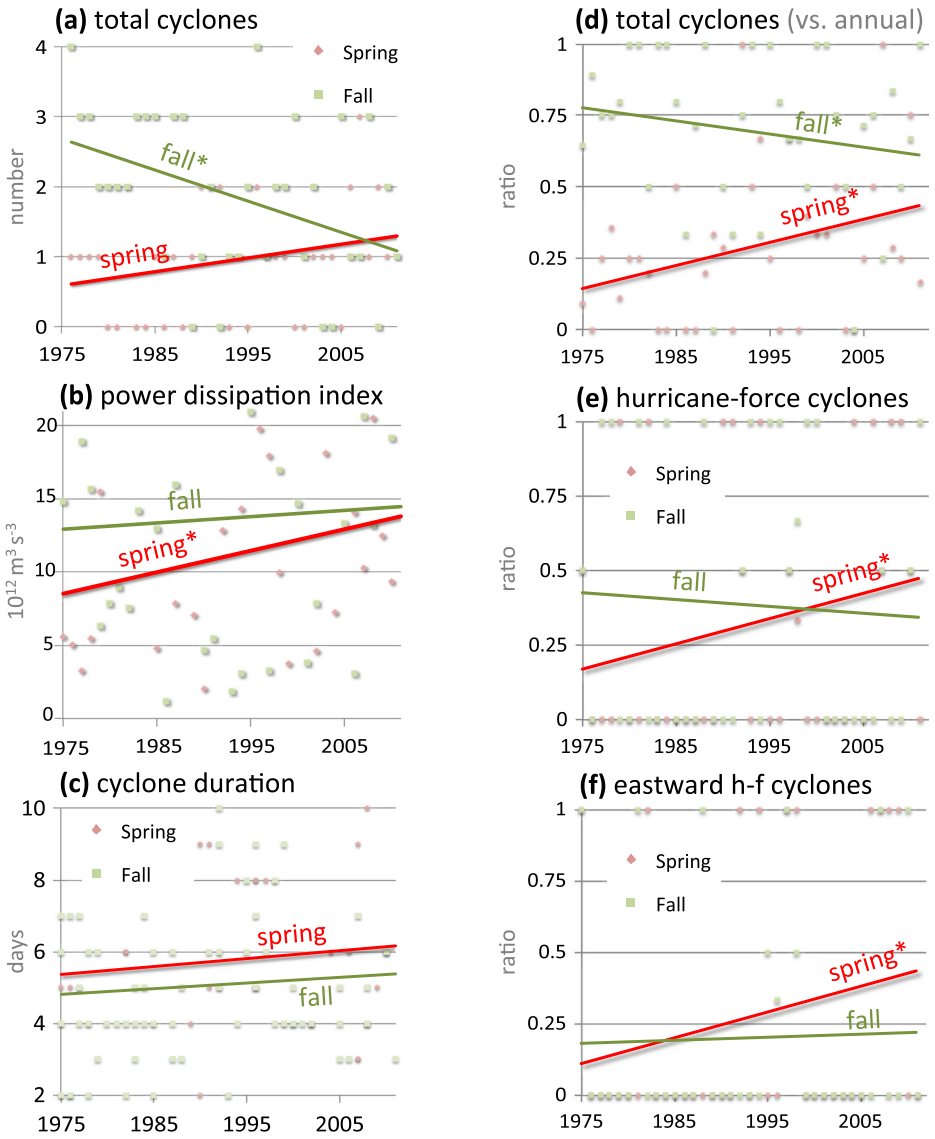

Figure 2. Bay of Bengal tropical cyclone (a) Number, (b) PDI, and (c) duration in spring (red) and fall (green) and linear trends over the 1976–2011 period. (d) Ratio of annual TC counts with spring and fall counts. (e) Ratio of annual hurricane-force TC counts in the BOB with spring and fall counts. (f) Ratio of annual hurricane-force TCs that moved eastward or northeastward towards Myanmar or Bangladesh with those in spring and fall. Linear trends with * are significant at the 95% confidence level.

utilized the ERA-40 reanalysis [*Uppala et al.*, 2005]. For the gridded precipitation datasets, we used the GPCP [*Adler et al.*, 2003], CMAP [*Xie and Arkin*, 1997], GPCC (http://gpcc.dwd.de/), University of Delaware or UDEL [*Legates and Willmott*, 1990], PREC/L [*Chen et al.*, 2002], CRU [*Mitchell and Jones*, 2005], and APHRODITE [*Yatagai et al.*, 2012], and again the acronym, full name, and spatial resolution for each of these precipitation datasets are provided in Table 2. We also utilized the NOAA Optimum Interpolation Sea Surface Temperature (SST) version 2 data at weekly intervals, that begins in 1981 [*Reynolds et al.*, 2002], and the monthly Extended Reconstructed (ER) SST that begins in 1950 [*Smith and Reynolds*, 2003]. The TC best track records were obtained from the Joint Typhoon Warning Center (JTWC) at their webpage http://www.usno.navy.mil/NOOC/nmfc-ph/RSS/jtwc/best_tracks/ioindex.html.

[7] In an attempt to attribute the cause(s) of the observed changes in circulation and TC activity over the BOB, we examined historical simulations of the Community Earth System Model (CESM), the latest generation of the fully coupled, community climate model [*Hurrell et al.*, 2013]. These CESM experiments were produced for the fifth phase of the Coupled Model Intercomparison Project (CMIP5) [*Taylor et al.*, 2011] and used four CMIP5 sets of historical single-forcing experiments that are driven by (a) natural forcing only (Natural, including solar and volcano), (b) aerosol forcing only (Aerosol), (c) greenhouse gas forcing only (GHG), and (d) all forcing combined (Historical). Each experiment produced a two-member ensemble initialized

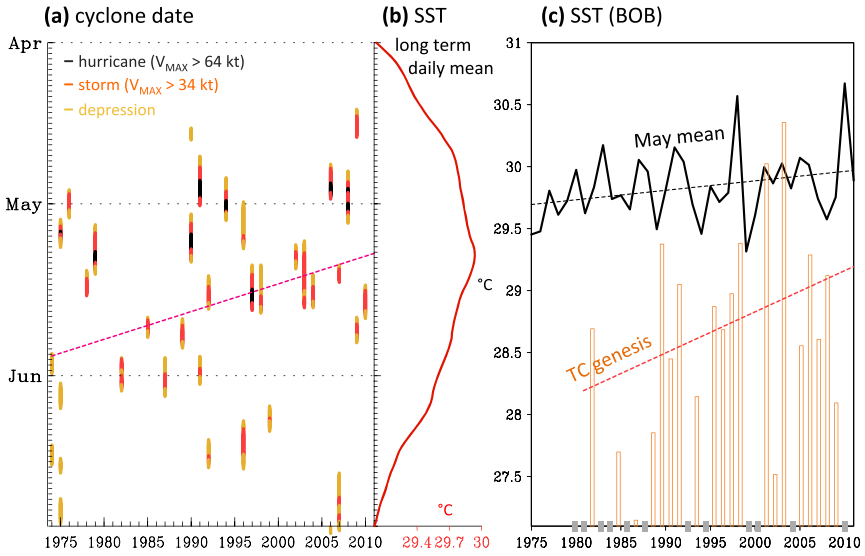

Figure 3. (a) TC occurrence dates colored for different stages of intensity superimposed with the linear trend. (b) Climatological daily SST in the BOB averaged over the 80°–95°E, 5°–20°N domain. (c) May SST in the BOB (black line) and SST during the week of spring TC genesis (orange bar) over the same region as in Figure 3b, added with respective linear trends.

from long-stable preindustrial (1850) control settings up to 2005.

3. Trends in Cyclones and SST

[8] TCs in the BOB have experienced changes between spring (April-June) and fall (September-November) since 1976, a time when reliable satellite observation became available [*Reynolds et al.*, 2002]. As shown in Figure 2a, the number of spring cyclones has increased slightly (+0.7 during 35 years) while fall cyclones have decreased significantly (−1.6). Hereinafter, the word "significant" is determined by $p < 0.05$. To examine changes in the potential destructiveness of TCs over time, we computed the power dissipation index (PDI) as introduced by *Emanuel* [2005]:

$$\mathrm{PDI} \equiv \int_0^{\tau} V_{\max}^3 \, \mathrm{dt}, \qquad (1)$$

where V_{max} is the maximum sustained wind speed and τ is the lifetime of a TC. The PDI provides a preferable measure of TC threat over the use of storm frequency or intensity alone. The trends in PDI (Figure 2b) indicate a significant increase in spring and a slight increase in fall, signifying the intensification of spring TCs. Since the PDI is also a function of TC lifespan, Figure 2c shows that cyclone durations have increased slightly, with spring (fall) TCs being lengthened about 0.6 day (0.4 day).

[9] Next, we used the *ratio* between seasonal and annual measures to summarize the contrasting changes in TC activity during the two seasons. It was found that the seasonal ratio of TC counts versus the annual total has increased in spring but decreased in fall (Figure 2d). Meanwhile, the ratio of TCs that grew to hurricane force (of category-1 or greater) has doubled in spring but decreased in fall (Figure 2e). Furthermore, the ratio of hurricane-force TCs that turned eastward and made landfall in either Myanmar or Bangladesh has doubled in spring but remains unchanged in fall (Figure 2f). The consistent and significant upward trend of spring TCs in Figures 2d–f suggests that cyclones developed in the BOB have become more likely to grow into hurricane force and more likely to strike Myanmar and Bangladesh.

[10] The occurrence dates of spring TCs were also examined and are plotted in Figure 3a overlaid with intensity. A pronounced advancement in the TC occurrence dates is revealed, amounting to about 10 days, changing from the last week of May in the late 1970s into the second week of May after 2005. This advancement in TC dates is coincident with the advancing monsoon onset in the region [*Kajikawa et al.*, 2012]. The frequency of severe cyclones ($V_{max} > 64$ kts) appears to be increasing, consistent with Figure 2b. When compared with climatological daily mean SST in the BOB (80°–95°E, 5°–20°N) shown in Figure 3b, TCs have occurred earlier in the season, and their occurrences have become more coincident with the seasonal maximum of SSTs - in the second week of May. The combined impact is shown in Figure 3c: while May SST in the BOB has only increased by 0.3 °C from 1975 to 2011, SST during TC geneses has increased by 1 °C (i.e., computed from weekly SST data over the 80°–95°E, 5°–20°N region during the week of TC genesis). These SST changes suggest that the warming of seasonal mean SST in the BOB may not play a direct role in the intensification of TCs.

4. Changes in Environmental Factors

4.1. Moisture Transports and Precipitation

[11] In this section, we will focus on the spring (premonsoon) season and study the extent to which the anomalous circulations lead to the observed increase and intensification of TCs. We computed the linear trends of the 850-mb wind and relative vorticity fields for May over the period of 1979–2010. As shown in Figures 4a–c, all

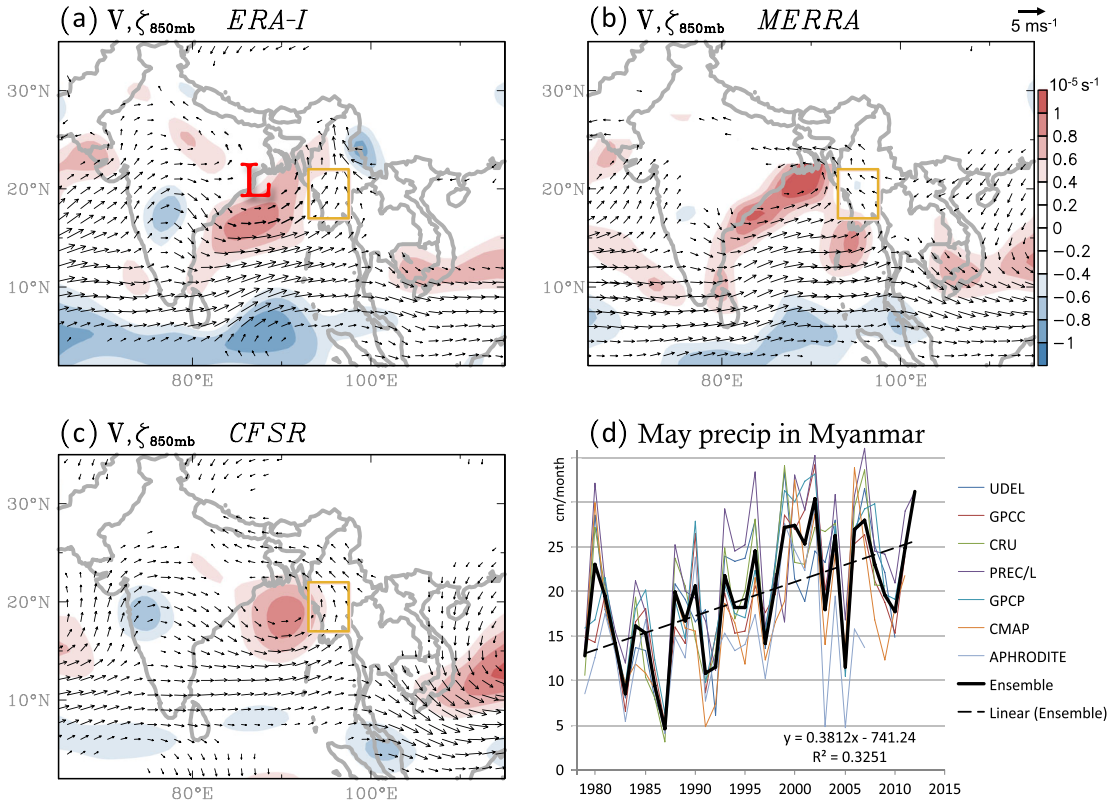

Figure 4. Horizontal distributions of linear trends of the 850-mb winds (**V**; vector) and relative vorticity (ζ; shadings) for May during the 1979–2010 period from (a) ERA-Interim, (b) MERRA, and (c) CFSR. Trends of **V** plotted are significant above the 90% level per *t*-test. (d) May precipitation series from all seven datasets (thin lines) and their ensemble mean (thick line) averaged over western Myanmar within the golden box in the maps. The trend formula was derived from the ensemble mean.

three reanalysis products fully capture the BOB monsoon trough intensification over this timespan, though each reanalysis portrays the trough intensification somewhat differently. For instance, the deepened trough in CFSR is closer to Myanmar than that in MERRA, but MERRA does not depict the deepened trough over the Indo-Gangetic Plain, which is manifest in ERA-Interim and CFSR. The deepened trough in the Indo-Gangetic Plain is a known response to the local premonsoon warming, which has been attributed to increased loading of anthropogenic absorbing aerosols, mainly black carbon [*Gautam et al*., 2009; *Ganguly et al*., 2012]. Regardless of the subtle differences, all three reanalysis products indicate enhanced southwesterly winds towards Myanmar associated with the depended monsoon trough. This result echoes *Kajikawa et al*. [2012] who, based solely on the NCEP2 Reanalysis data [*Kanamitsu et al*., 2002], showed that the premonsoon circulation over the South Asia-Western Pacific region has intensified towards a more developed monsoon structure.

[12] We next examined changes in May precipitation over western Myanmar, the domain of which is outlined in Figure 4. Myanmar undergoes its highest TC frequency in May, which is also the monsoon onset month [*Sen Roy and Kaur*, 2000]. The domain averages of May precipitation from the seven precipitation datasets are shown in Figure 4d and overlaid with ensemble means and linear trends. The spatial resolution of each dataset was interpolated to 1.0° prior to averaging. Despite the slight disagreement of interannual variability among different datasets, there is a significant upward trend for all seven datasets, indicating that May precipitation in western Myanmar has doubled in total amount. *Kajikawa et al*. [2012] also demonstrated that May precipitation around the BOB increased while June (post-onset) precipitation decreased since 1979. These changes together indicate an advanced, more energized premonsoon (and a longer monsoon) season for the BOB and Myanmar.

[13] We also explored the extent to which the intensified BOB monsoon trough may facilitate increases in TC intensity, by examining the moisture transport. In order to depict the precipitation maintenance process, we followed *Yoon and Chen* [2005]'s water vapor budget analysis for the Indian monsoon depression, by computing the SF and potential function of the column-integrated water vapor flux, **Q**, referred to as *SFQ* and *VPQ* respectively:

$$SFQ = \nabla^{-2}\left(\vec{k}\cdot\nabla\times\mathbf{Q}\right) \tag{2}$$

and

$$VPQ = \nabla^{-2}(\nabla\cdot\mathbf{Q}). \tag{3}$$

[14] The rotational (divergent) components of **Q** were then derived from the curl (gradient) of *SFQ* (*VPQ*), denoted as $\mathbf{Q}_R$ and $\mathbf{Q}_D$, respectively. Given the slightly different

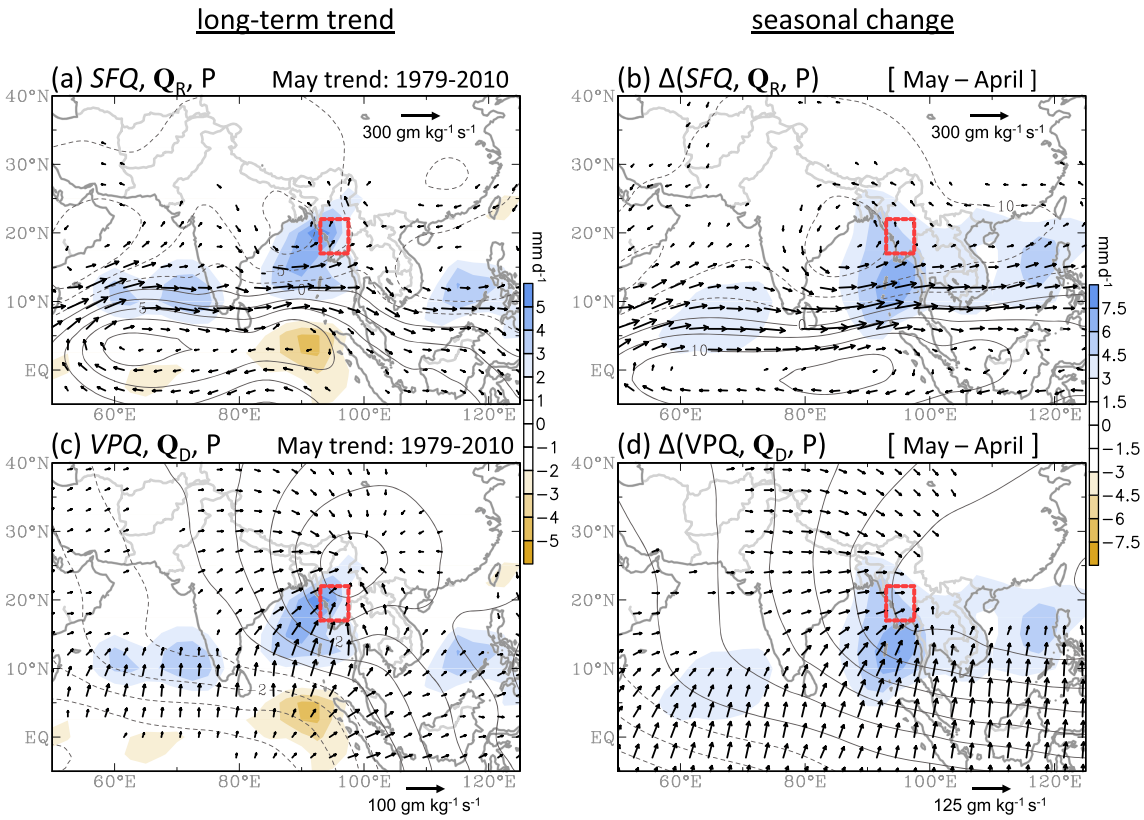

Figure 5. Linear trends of precipitation (shadings) and (a) SFQ (contours) and $\mathbf{Q}_R$ vectors, as well as (c) VPQ and $\mathbf{Q}_D$ in May for the 1979–2010 period, using the three-reanalysis ensemble data. The vectors and shadings are generally significant at the 90% level. Units are converted to per 32 years since 1979. Figures 5b and 5d are similar to Figures 5a and 5c except for the monthly differences between May and April indicating the seasonal progression of the moist flux circulations and precipitation. Western Myanmar is outlined by a red box.

circulation changes depicted by the different reanalyses (Figure 4), an ensemble average of these reanalyses was used at 1.5° × 1.5° spatial resolution.

[15] The linear trends of *SFQ* (Figure 5a) in May reveal a robust cyclonic circulation over the BOB that is consistent with the 850-mb wind pattern (Figure 4). The precipitation shown here was computed from the average of GPCP and CMAP to cover the oceans, and their trends exhibit a north-south stratification across ~10°N. Increased precipitation collocates with the westerly fluxes in the southern Arabian Sea and is further enhanced over the BOB and Myanmar. Decreased precipitation is distributed within the anticyclonic cell off the equator. Notably, this tendency of *SFQ* resembles the climatological monsoon onset (or transition) of *SFQ* from April to May, which is shown in Figure 5b. Both circulation anomalies depict a prominent trough developed over the BOB transporting moisture towards Myanmar. This marked correspondence between the 32-year trends and the climatological onset pattern is suggestive of a strengthened, more rapid monsoon transition leading to enhanced moisture supply into the BOB and over Myanmar.

[16] According to the water vapor budget equation, only the divergent component of the water vapor flux directly contributes to the precipitation process (i.e., water vapor source/sink), so we therefore computed the linear trends of *VPQ* (Figure 5c). A convergence center covers northern Myanmar and Bangladesh, accompanied by a northeast-southwest oriented convergence band of the water vapor flux over the BOB, indicating an increase in moisture pooling that contributes to increasing precipitation. Fluxes of $\mathbf{Q}_D$ also converge towards the westerly zone of $\mathbf{Q}_R$ parallel to and north of the equator, supporting the anomalous precipitation belt along 10°N. Since *SFQ* and *VPQ* mainly reflect the lower-tropospheric circulations, the cyclonic *SFQ* illustrates the deepening of the monsoon trough while the divergent *VPQ* indicates enhanced low-level convergence east of the trough. Moreover, the *VPQ* trends also resemble the April-to-May transition (Figure 5d) as both portray the increased convergence of moisture fluxes towards the BOB and Indochina from the Southern Hemisphere. This again suggests a stronger, more rapid moistening process associated with the monsoon transition in May, with large precipitation increases in the BOB and Myanmar being the consequence.

[17] Using the daily APHRODITE precipitation data up to 2007, we estimated the contribution of TCs to the precipitation in Myanmar (domain outlined in Figure 5). This was done by accumulating precipitation during the days when any TC center moved to within 200 km of and/or over Myanmar. It was found that TCs contribute to 12.3% of precipitation in May over Myanmar for the period of

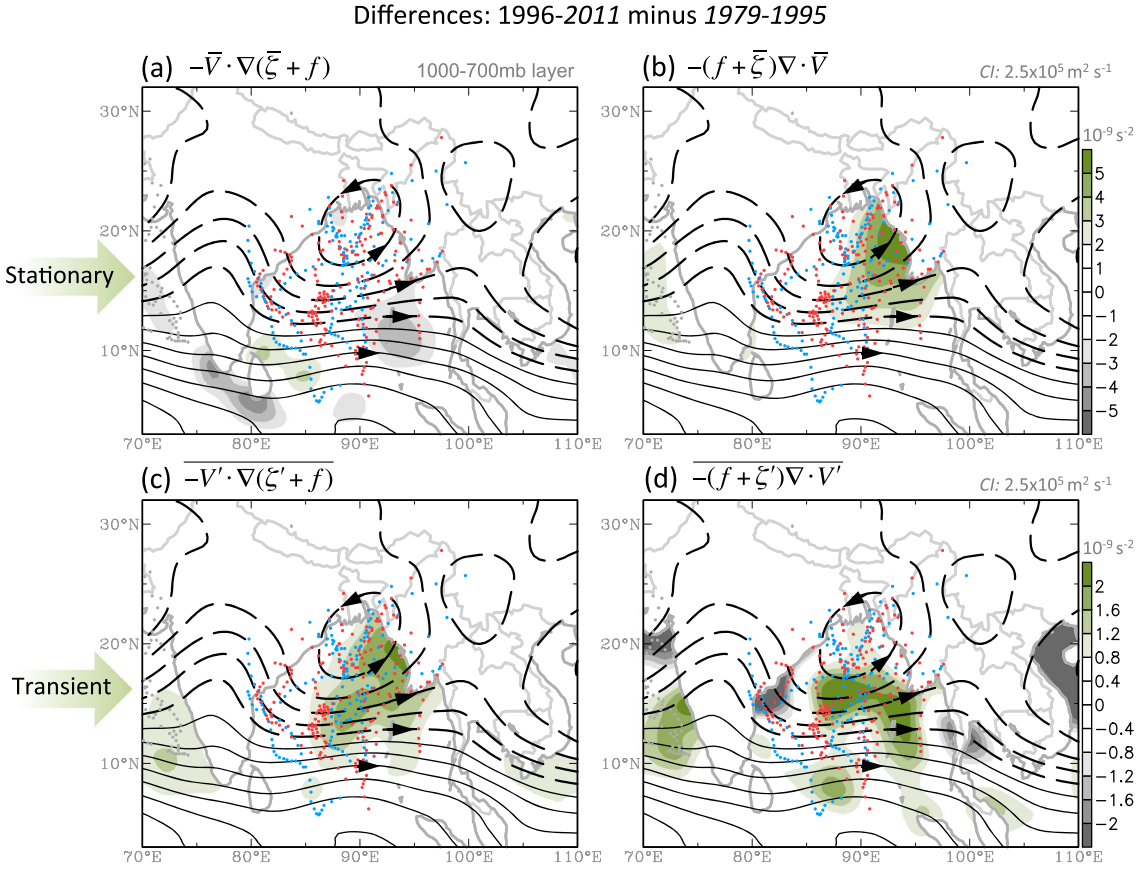

Figure 6. The 15-year difference between 1996–2011 and 1979–1995 from the vorticity generation of (a) total vorticity advection and (b) total vortex stretching (shadings) overlaid with the difference in 850-mb streamfunction (contours) and 6-h TC tracks (dots). For TC tracks, red (blue) dots indicate the 1996–2011 (1979–1995) period of 6-h locations after reaching tropical storm winds (> 34 kts). Figures 6c and 6d same as Figures 6a and 6b but for the differences in the transient activity of the vorticity generation terms. The vorticity budget over land was masked for the consideration that TCs only form and grow over the ocean.

1975–2007 (as limited by the data length of APHRODITE and hence excluding the contribution of cyclone Nargis in 2008). This TC-related precipitation fraction also exhibits an increase (not shown) with a trend approximately two thirds of the increase in May precipitation. Thus, the increased May precipitation over Myanmar is contributed to by at least two sources: (a) increased monsoonal moisture being directed towards Myanmar due to the deepened trough and (b) intensified TCs and their pro-eastward movement per Figure 2f.

4.2. Vorticity Dynamics

[18] The dynamical processes that link the intensified BOB monsoon trough to the changes in spring TCs were examined further by computing the vorticity budget for the lower troposphere, consisting of the 1000, 925, 850, 700, and 600-mb pressure levels. The horizontal wind fields (**V**) were integrated from these five levels prior to calculation of the vorticity budget equation,

$$\frac{\partial\zeta}{\partial t}\approx -V\cdot\nabla(\zeta+f)-(\zeta+f)\nabla\cdot V, \tag{4}$$

where ζ is relative vorticity and f is the Coriolis parameter. This equation can be decomposed into two modes: stationary (first right term below) and transient (second right term below),

$$-V\cdot\nabla(\zeta+f)=-\bar{V}\cdot\nabla\left(\bar{\zeta}+f\right)-\overline{V'\cdot\nabla(\zeta'+f)} \tag{5}$$

and

$$-(\zeta+f)\nabla\cdot V=-\left(\bar{\zeta}+f\right)\nabla\cdot\bar{V}-\overline{(\zeta'+f)\nabla\cdot V'}\ . \tag{6}$$

For the time-mean circulations, vorticity tendency $\frac{\partial\zeta}{\partial t}$ was assumed to be zero, and the tilting term is small enough to be neglected. Shown in Figure 6a is the difference in stationary vorticity advection $-\bar{V}\cdot\nabla\left(\bar{\zeta}+f\right)$ between the 2011–1996 era and the 1979–1995 era, superimposed with the difference in the 850-mb SF that depicts the intensified monsoon trough. The change in vorticity advection is weak, and overall is negative over the BOB due to planetary vorticity advection (not shown). Meanwhile, the difference in stationary vortex stretching $-\left(\bar{\zeta}+f\right)\nabla\cdot\bar{V}$ (Figure 6b) exhibits a widespread intensification that covers the eastern BOB and Myanmar. This points to strengthening of low-level vorticity generation as a result of enhanced vortex stretching in the environmental flows. Notably, the area of enhanced vortex stretching also covers most of the eastward TC tracks that only appeared after 1995.

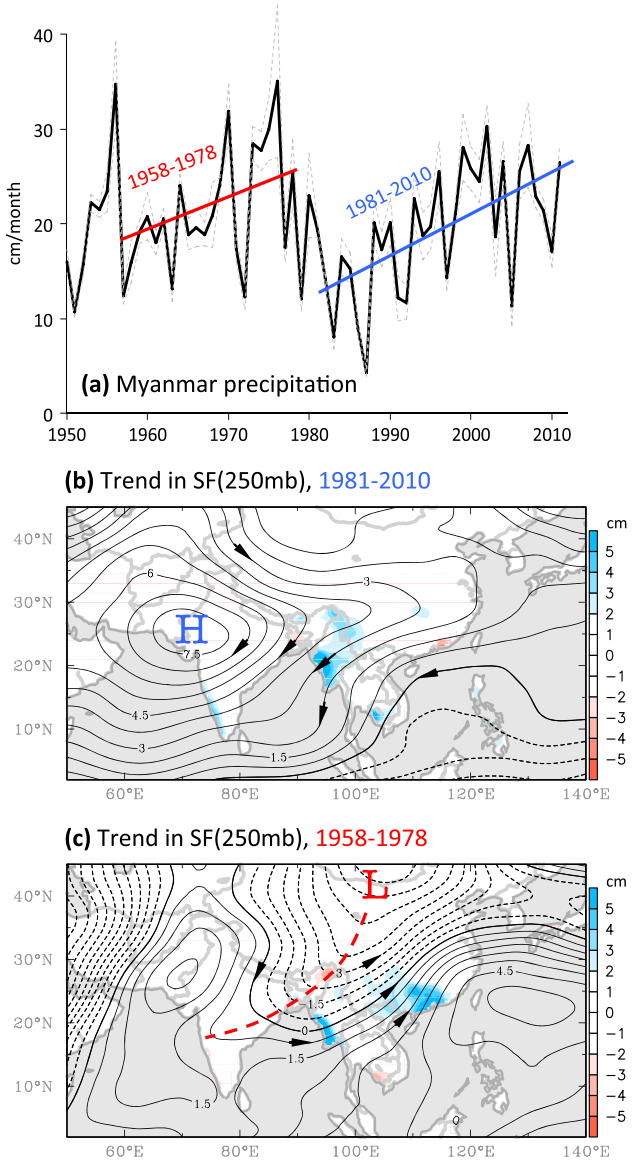

Figure 7. (a) May precipitation ensemble over Myanmar since 1950, overlaid with linear trends for the two periods as indicated, and the range of one standard deviation (light gray dashed lines). (b) Horizontal distribution of linear trends of the 250-mb streamfunction and precipitation in May over the 1981–2010 period, in which "H" indicates the anticyclonic anomaly. Figure 7c same as Figure 7b but for the 1958–1978 period, marked by "L" and red dashed line to indicate the deepened trough extending from the midlatitudes.

[19] Under prevalent ambient flows, TC movement is mainly steered by vorticity advection in the middle-to-lower troposphere [e.g., *Carr and Elsberry*, 1990; *Chen et al.*, 2009]. Thus, the weak anomalies of stationary vorticity advection (Figure 6a) seem contradictory to the tendency for eastward-moving TCs. To examine further, we displayed in Figure 6c the difference in transient vorticity advection $-\overline{V'\cdot\nabla(\xi'+f)}$. A marked increase over the BOB is found for the southern and eastern periphery of the intensified monsoon trough. This result indicates increased advection associated with any synoptic disturbances, including TCs, for them to move eastward and thus towards Myanmar. This result also substantiates the steering effect of the enhanced southwesterly flows on individual storms. Notably, the difference in transient vortex stretching $-\overline{(\zeta'+f)\nabla\cdot V'}$ (Figure 6d), also shows intensification near Myanmar, suggesting deflected tracks of TCs with increased intensity. These analyses outline favorable environmental conditions (i.e., the deepened monsoon trough) for the development and eastward movement of TCs.

4.3. Low-Frequency Variability

[20] Multidecadal climate variability in the BOB monsoon has been observed, such as the Pacific Decadal Oscillation that modulates the summer precipitation over Myanmar [*Roy and Roy*, 2011], and a significant 38–68 years signal of monsoon variations found in Myanmar's teak tree rings [*D'Arrigo et al.*, 2011]. It is therefore prudent to examine the extent to which such multidecadal variability impacts the post-1979 change in precipitation. Thus, May precipitation for Myanmar was extended back to 1950 and is displayed in Figure 7a, with the exclusion of the GPCP and CMAP data in the ensemble records. We used the year of 1950 as a starting point because only two precipitation datasets (UDEL and CRU) were available prior to this date, and data uniformity before World War II is questionable.

[21] Two distinct periods with significant increases of May precipitation were identified in Figure 7a. We computed the linear trends in the upper-level (250-mb) SF for these two periods of marked precipitation increase: 1958–1978 versus 1981–2010 (determined because they exhibit the greatest upward trends over a period of 20 years or longer throughout the analysis period). These SF trends were computed from ERA40 for the earlier (pre-1979) era and from ensemble reanalysis for the latter era. The pre-1979 precipitation increase actually began in the early 1950s, but we started with 1958 due to the limitation of ERA40. Noteworthy is that the 1958–1978 precipitation increase has also been reported for central Myanmar [*Sen Roy and Kaur*, 2000]. As shown in Figures 7b and c, the trends in the upper-level circulations are very different between the two eras, even though they both are linked to increased precipitation in Myanmar.

[22] During the modern era of 1981–2010 (Figure 7b), the extensive anticyclonic anomaly over South Asia signified intensification of the monsoon high in the premonsoon season (trends in the 1979–2010 period are very similar). Together with the intensified monsoon trough at lower levels (Figure 6), the troposphere over South Asia has evidently expanded, and this occurs in association with a stronger and faster monsoon development. In contrast, a very different circulation pattern appeared from the 1958–1978 era (Figure 7c), which is characterized by a deep baroclinic trough extending from Siberia to the BOB. The low-level circulation trends (not shown) depict a weak cyclonic cell centered at Bangladesh that corresponds to the upper-level trough. Located in the southeastern tip of this trough, both Myanmar and southern China experienced increased precipitation. Because the premonsoon season in this region did undergo midlatitude influences [*Htway and Matsumoto*, 2011], the circulation difference between Figures 7b and

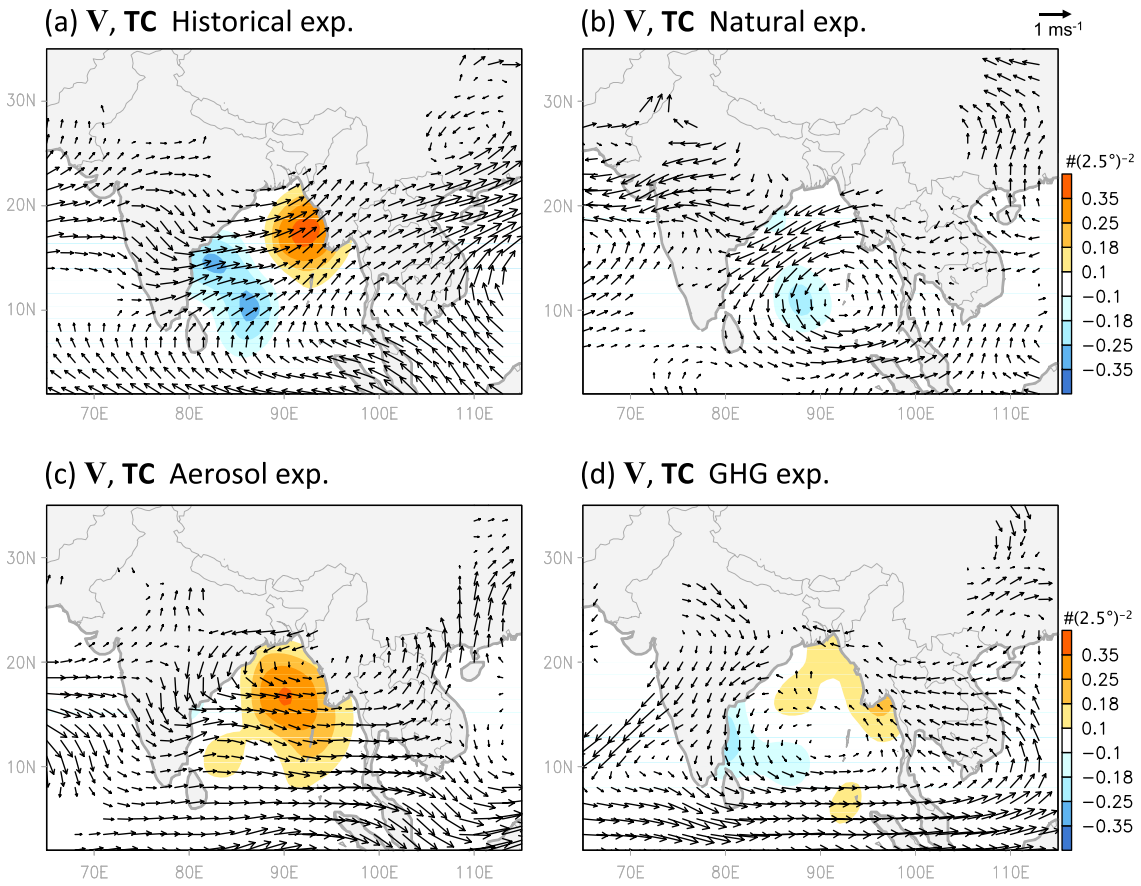

Figure 8. Same as Figure 4 but with the linear trends of May 850-mb winds (vectors) and the areal frequency of spring TCs (shadings; see text) during the 1974–2005 period as simulated by the CESM single-forcing experiments. Unit is converted to per 32 years.

7c is highly suggestive that Myanmar's premonsoon climate may have experienced a regime change, from an apparent midlatitude circulation regime to a tropical/monsoonal one. Moreover, such contrasting circulation patterns that resulted in similar precipitation increases contradict the possibility of any systematic modulation from lower-frequency variability.

4.4. Roles of Vertical Shear and SST

[23] Intriguingly, the upper-level circulation trends during the modern era (Figure 7b) portray a dynamical difference of the increased TC intensity between the BOB and the Arabian Sea. In the case of the BOB, the deepened monsoon trough at the lower levels and the northeasterly anomalies at the upper levels together enhanced vertical easterly shear. However, enhanced easterly shear is climatologically unfavorable to TC development [*Hoarau et al*., 2011; *Ng and Chan*, 2012]. In the case of the Arabian Sea, the observed increases in TC genesis and intensity have been attributed to weakened vertical shear in both the pre- and postmonsoon seasons [*Evan et al*., 2011]. The fact that vertical shear has enhanced over the BOB seems contradictory to the observed increase in TC intensity.

[24] Earlier studies [e.g., *Pattanaik*, 2005; *Chan*, 2007] argued that TC activity in the northern Indian Ocean is primarily affected by variability of the atmospheric circulation rather than SST. However, the contribution of SST warming cannot be ruled out here because, in the BOB, the seasonal SST reaches its maximum in May (Figure 3b). Thus, even though SST in the northern Indian Ocean has warmed rather homogeneously throughout the year, the average 0.4 °C warming on top of the average 29.7 °C in May has pushed SST to exceed 30 °C since the late 1990s (Figure 3c). We suggest here, that such warm SST combined with strengthened lower-tropospheric vorticity generation and moisture pooling are crucial factors for the increases in TC number and intensity over the BOB.

5. CESM Attribution Analysis

[25] Recent research [e.g., *Lau and Kim*, 2006; *Gautam et al*., 2009; *Ganguly et al*., 2012] has suggested that, since the 1970s, anthropogenic influences from absorbing aerosols (including black carbon and dust) played a major role in heating the troposphere over South Asia. To examine, we computed the linear trends in the CESM model 850-mb winds following the analysis in Figure 4, but using a comparable 32-year period of 1974–2005 due to the data limit of CESM. The Historical experiment (Figure 8a) depicted the deepened trough over the northern BOB, and this simulated circulation pattern is very similar with that observed, especially with MERRA (see Figure 4b). Prevailing increases in the southwesterly flows were found over Myanmar and much of the Indochina Peninsula. Such circulation features were not depicted by the Natural experiment (Figure 8b) in

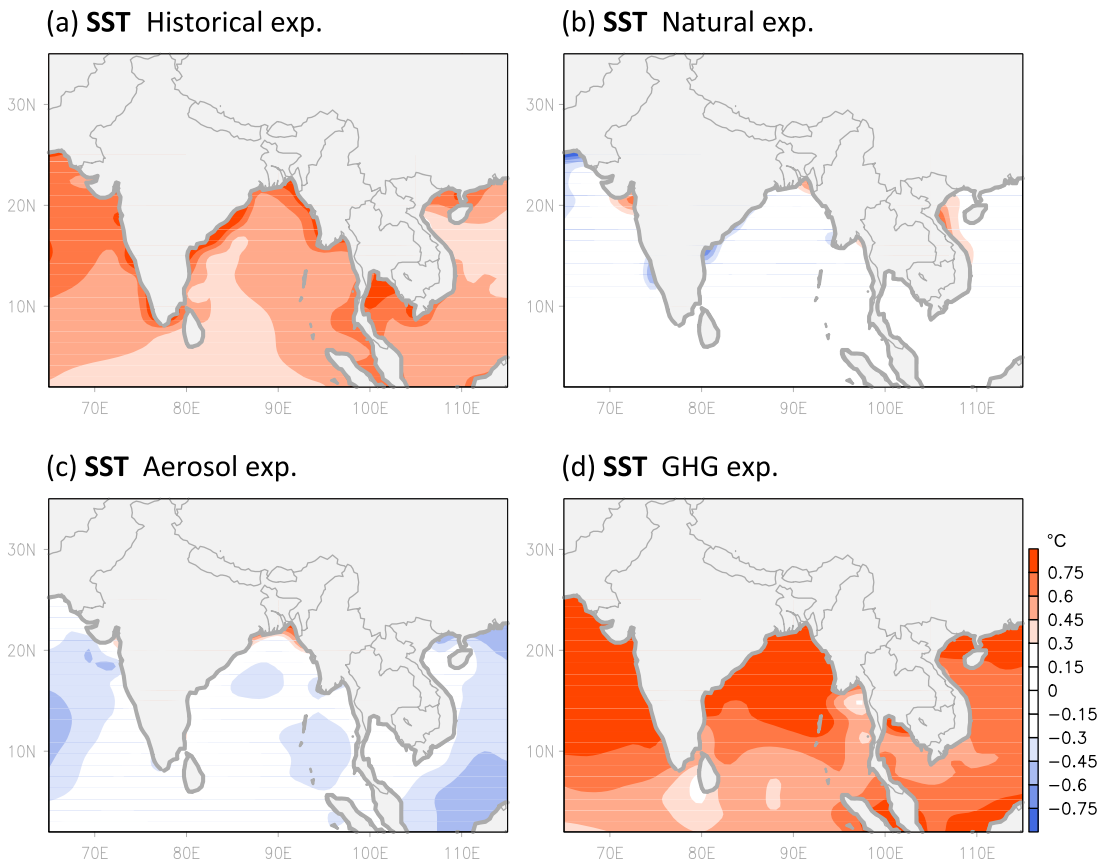

Figure 9. Same as Figure 8 but with the May trends of SST simulated by the CESM single-forcing experiments. Unit is converted to per 32 years.

which northeasterly trends dominate the northern BOB with anticyclonic circulation over northern India. However, in the Aerosol experiment (Figure 8c), the monsoon trough was much intensified, and particularly so for the northern BOB along the eastern Indian coast. The GHG experiment (Figure 8d) revealed a similar but weaker intensification of the monsoon trough at a broader scale over the entire BOB, without the local deepening of the monsoon trough as was seen in the observation.

[26] These simulated circulation anomalies therefore support earlier studies [*Lau and Kim*, 2006; *Gautam et al.*, 2009; *Bollasina et al.*, 2008] that the recent warming trend in the troposphere over the South Asian monsoon region is most prominent in the premonsoon season with the maximum warmth occurring in May. There are a couple of different hypothesized pathways that absorbing aerosols can follow to enhance premonsoon heating. One pathway is through heating by increased dust and soot aerosol loading along the Himalaya-Tibetan Plateau leading to increase in the meridional thermal contrast [*Lau and Kim*, 2006]. The other pathway is through a semi-direct effect of clouds of smoke generated by anthropogenic burning that has warmed the lower troposphere [*Bollasina et al.*, 2008]. Regardless, the result is the intensification of monsoon transition, which in turn causes the circulation pattern in May to become more like that in June [*Kajikawa et al.*, 2012]. Embedded in such circulation change, the BOB monsoon trough has deepened correspondingly, as simulated by the CESM Aerosol experiment.

[27] Next, we attempted to examine the direct linkage between TCs and the anomalous circulations, by using the daily mean sea level pressure (MSLP) output from the CESM. The first step in our algorithm was to define MSLP minimum, computed by the Laplacian of MSLP at each grid point using centered differencing [*Davis et al.*, 2002]. The Laplacian must be positive to pass the first stage of the algorithm, and this starting condition allows for detection of MSLP anomalies embedded within large-scale pressure gradients. In order to focus on TC-like vorticities or low-pressure centers, it is desirable to filter out larger-scale systems that are the essentially the monsoon troughs. To filter these out we (a) performed spatial harmonic analysis restricting the diameter (zonal dimension) of low-pressure cells to be less than 1500 km and (b) computed MSLP tendency over 24 h in order to determine whether or not a continuous track of the MSLP anomaly is present (i.e., eliminating stationary low-pressure systems such as the monsoon trough). For the second criterion, negative MSLP tendency during the lifecycle of a probable TC must be present and exceed 2 mb for at least two consecutive days. Manual tracking was performed for this second criterion. Cyclones were traced from April to June for the 1974–2005 period in each of the two members of CESM experiment. The areal frequency of TCs was then projected onto a $2.5° \times 2.5°$ grid mesh for spatial analysis.

[28] The linear trends of TC areal frequency were computed and are overlaid with the wind anomalies in Figure 8. In the Historical experiment, the change in TC frequency

exhibits a dipole pattern with pronounced increases in the northeastern BOB and decreases in the southwestern BOB (Figure 8a). This tendency echoes the observed increase in eastward-moving TCs (see Figure 6). However, only the Aerosol experiment produced the overall increase of TCs in the BOB (Figure 8c), which corresponds to the deepened trough. The GHG experiment revealed a similar but weaker dipole of the TC frequency trends (Figure 8d), while the Natural experiment only depicted weak, negative trends associated with the anticyclonic anomalies. These CESM experiments are therefore suggestive that the deepened monsoon trough favors cyclone formation *and* eastward propagation. Under such conditions, the lower-tropospheric dynamics appear to dominate, and possibly offset, the enhanced vertical shear that acts to reduce TC formation (section 4.4). This dynamical process is apparently different from the role of decreased vertical shear in the Arabian Sea TCs as was claimed by *Evan et al*. [2011]; rather, it seems supportive of the increased land-sea temperature contrasts leading to stronger moisture convergence as was argued by *Wang et al*. [2012].

[29] Simulations of the CESM also revealed an SST warming trend in the BOB (Figure 9a) close to that observed (Figure 3c). With the single-forcing experiments, the overall warming appears to be overwhelmingly caused by the GHG forcing (Figure 9d), but this is likely offset by weak sea surface cooling associated with the Aerosol experiment due to reduced solar radiation (Figure 9c). The Natural experiment did not create any substantial changes in SST (Figure 9b), suggesting that the observed SST trend in this region results mainly from anthropogenic activities. Therefore, while anthropogenic aerosols might have caused the increases in TC frequency and eastward movement through tropospheric warming and deepening of the monsoon trough, the GHG forcing may further contribute to the increased TC power through SST warming.

6. Concluding Remarks

[30] Based upon ensembles of global reanalyses and precipitation datasets, we demonstrate a robust intensification of the May monsoon trough over the BOB since 1979, with a corresponding increase in precipitation over Myanmar and a modulation of spring TCs. The result has been more intense cyclones in general, and an increase in the number of TCs that impacted Myanmar. The precipitation increase was not unprecedented. For example, during the 1958–1978 period, Myanmar underwent a similar increase in May precipitation, but the increase was caused by a deepening of midlatitude troughs. In contrast, the post-1979 increase in premonsoon precipitation was a result of enhanced monsoonal circulation in South Asia, evidenced by the lower-level cyclonic and upper-level anticyclonic anomalies that reflect tropospheric expansion—i.e. warming. Such circulation changes in the premonsoon season have deepened the BOB monsoon trough and led to a tendency that TCs are occurring earlier each year. The deepened monsoon trough also affected the frequency and track of TCs in the BOB. Such a change in premonsoon circulation has been attributed to atmospheric warming caused by increased anthropogenic aerosols in the Indo-Gangetic Plain. Analyses of the CESM single-forcing experiments provide further evidence for the effect of aerosols on the deepening of the BOB monsoon trough and the resulting increases in TC frequency, intensity, and trajectory.

[31] Caution, however, should be taken in interpreting the modeling results. The CESM produced a spring TC frequency that was too evenly distributed over the April-June season (not shown) compared to the concentrated frequency in May in the observation. Further, although the CESM simulated the large-scale circulation and SST changes very closely to that which was observed, rainfall was poorly simulated (not shown). The CESM severely underestimated precipitation during the premonsoon season of April and May and simulated the precipitation center too far to the north. Such bias is likely caused by the rather coarse (2-degee) grid spacing of the CESM being unable to capture the fine-scale orographic effect on precipitation over Myanmar, where steep and narrow mountains greatly affect the precipitation climatology [*Sen Roy and Kaur*, 2000]. Therefore, further studies using limited-area models or high-resolution global models are preferred to link simulated circulation patterns to precipitation anomalies. A further examination of TC occurrences is also needed in order to establish a more direct cause-and-effect relationship between anthropogenic activity and changing TC activity, a relationship that would be most effectively realized through fine-resolution climate modeling.

[32] In the meantime, a careful evaluation of historical simulations from other climate models, such as those participating in the CMIP5, is necessary since (a) most of global climate models have difficulty in simulating TCs due to coarse spatial scale (~100 km), and (b) even with a global climate model that has exceptionally higher spatial resolution, *Murakami et al*. [2012] have demonstrated the challenge associated with simulating spring TC frequency in the northern Indian Ocean. A possible way of getting around this situation is by engaging regional climate models to produce so-called "downscaling simulation" in order to capture the fine scale of TCs under the changing large-scale circulations and SST. A test of embedding a regional climate model within the CESM to simulate TCs in the northern Indian Ocean is actively being undertaken.

[33] Finally, because anthropogenic aerosol loading is projected to slowly decrease in contrast to steady increase of GHGs, and hence leading to complex responses in tropospheric temperature and SST, it would be prudent to examine future climate simulations for the premonsoon season climate for the BOB and Myanmar. Future research initiatives, such as those just described, will help develop disaster responding strategies for Myanmar and strengthen its societal resilience.

[34] **Acknowledgments.** Insightful suggestion from L. Ruby Leung at PNNL is highly appreciated. This study was supported by Grant NNX13AC37G, NSF GEO 09-08971, and the Utah State University Agricultural Experiment Station (approved as journal paper number 8503 and as Lamont-Doherty Contribution No. 7685). J.-H. Yoon was supported by Office of Science of the U.S. Department of Energy as part of the Robust regional modeling project. The Pacific Northwest National Laboratory is operated for DOE by Battelle Memorial Institute under contract DE-AC05-76RL01830.

References

Adler, R. F., et al. (2003), The Version-2 Global Precipitation Climatology Project (GPCP) Monthly Precipitation Analysis (1979–Present), *J. Hydrometeorology*, *4*, 1147–1167.

Bollasina, M., S. Nigam, and K. M. Lau (2008), Absorbing Aerosols and Summer Monsoon Evolution over South Asia: An Observational Portrayal, *J. Climate*, *21*, 3221–3239.

Carr, L. E., and R. L. Elsberry (1990), Observational Evidence for Predictions of Tropical Cyclone Propagation Relative to Environmental Steering, *J. Atmos. Sci.*, *47*, 542–546.

Chan, J. C. L. (2007), Interannual variations of intense typhoon activity, *Tellus A*, *59*, 455–460.

Chen, M., P. Xie, J. E. Janowiak, and P. A. Arkin (2002), Global Land Precipitation: A 50-yr Monthly Analysis Based on Gauge Observations, *J. Hydrometeorology*, *3*, 249–266.

Chen, T.-C., S.-Y. Wang, M.-C. Yen, and A. J. Clark (2009), Impact of the Intraseasonal Variability of the Western North Pacific Large-Scale Circulation on Tropical Cyclone Tracks, *Wea. Forecasting*, *24*, 646–666.

D'Arrigo, R., J. Palmer, C. C. Ummenhofer, N. N. Kyaw, and P. Krusic (2011), Three centuries of Myanmar monsoon climate variability inferred from teak tree rings, *Geophys. Res. Lett.*, *38*, L24705, doi:10.1029/2011GL049927.

Davis, C. A., D. A. Ahijevych, and S. B. Trier (2002), Detection and Prediction of Warm Season Midtropospheric Vortices by the Rapid Update Cycle, *Mon. Wea. Rev.*, *130*, 24–42.

Emanuel, K. (2005), Increasing destructiveness of tropical cyclones over the past 30 years, *Nature*, *436*, 686–688.

Evan, A. T., J. P. Kossin, C. E. Chung, and V. Ramanathan (2011), Arabian Sea tropical cyclones intensified by emissions of black carbon and other aerosols, *Nature*, *479*, 94–97.

Fasullo, J., and P. J. Webster (2003), A Hydrological Definition of Indian Monsoon Onset and Withdrawal, *J. Climate*, *16*, 3200–3211.

Ganguly, D., P. J. Rasch, H. Wang, and J.-H. Yoon (2012), Fast and slow responses of the South Asian monsoon system to anthropogenic aerosols, *Geophys. Res. Lett.*, *39*, L18804, doi:10.1029/2012GL053043.

Gautam, R., N. C. Hsu, K.-M. Lau, C.-S. Tsay, and M. Kafatos (2009), Enhanced pre-monsoon warming over the Himalayan-Gangetic region from 1979 to 2007, *Geophys. Res. Lett.*, *36*, L07704, doi:10.1029/2009GL037641.

Ghosh, S., V. Luniya, and A. Gupta (2009), Trend analysis of Indian summer monsoon rainfall at different spatial scales, *Atmos. Sci. Lett.*, *10*, 285–290.

Girishkumar, M. S., and M. Ravichandran (2012), The influences of ENSO on tropical cyclone activity in the Bay of Bengal during October– December, *J. Geophys. Res.*, *117*, C02033, doi:10.1029/2011JC007417.

Hoarau, K., J. Bernard, and L. Chalonge (2011), Intense tropical cyclone activities in the northern Indian Ocean, *Inter. J. Climatol.*, *32*, 1935–1945.

Hoarau, K., J. Bernard, and L. Chalonge (2012), Intense tropical cyclone activities in the northern Indian Ocean, *Inter. J. Climatol.*, *32*, 1935–1945.

Htway, O., and J. Matsumoto (2011), Climatological onset dates of summer monsoon over Myanmar, *Inter. J. Climatol.*, *31*, 382–393.

Hurrell, J. W., et al. (2013), The Community Earth System Model: A Framework for Collaborative Research, *Bull. Amer. Met. Soc.*, *117*, doi:10.1175/BAMS-D-12-00121.

Kajikawa, Y., T. Yasunari, S. Yoshida, and H. Fujinami (2012), Advanced Asian summer monsoon onset in recent decades, *Geophys. Res. Lett.*, *39*, L03803, doi:10.1029/2011GL050540.

Kanamitsu, M., W. Ebisuzaki, J. Woollen, S.-K. Yang, J. J. Hnilo, M. Fiorino, and G. L. Potter (2002), NCEP–DOE AMIP-II Reanalysis (R-2), *Bull. Amer. Meteor. Soc.*, *83*, 1631–1643.

Krishna, K. M. (2009), Intensifying tropical cyclones over the North Indian Ocean during summer monsoon—Global warming, *Global Planet. Change*, *65*, 12–16.

Krishnamurti, T. N., P. Ardanuy, Y. Ramanathan, and R. Pasch (1981), On the Onset Vortex of the Summer Monsoon, *Mon. Wea. Rev.*, *109*, 344–363.

Lau, K. M., and K. M. Kim (2006), Observational relationships between aerosol and Asian monsoon rainfall, and circulation, *Geophys. Res. Lett.*, *33*, L21810, doi:10.1029/2006GL027546.

Legates, D. R., and C. J. Willmott (1990), Mean seasonal and spatial variability in gauge-corrected, global precipitation, *Int. J. Climatol.*, *10*, 111–127.

Mitchell, T. D., and P. D. Jones (2005), An improved method of constructing a database of monthly climate observations and associated high-resolution grids, *Inter. J. Climatol.*, *25*, 693–712.

Murakami, H., et al. (2012), Future changes in tropical cyclone activity projected by the new high-resolution MRI-AGCM*, *J. Climate*, *25*, 3237–3260, doi:10.1175/JCLI-D-11-00415.1.

Ng, E. K. W., and J. C. L. Chan (2012), Interannual variations of tropical cyclone activity over the north Indian Ocean, *Inter. J. Climatol.*, *32*, 819–830.

Paltridge, G., A. Arking, and M. Pook (2009), Trends in middle- and upper-level tropospheric humidity from NCEP reanalysis data, *Theor. Appl. Climatol.*, *98*, 351–359.

Pattanaik, D. R. (2005), Variability of oceanic and atmospheric conditions during active and inactive periods of storms over the Indian region, *Inter. J. Climatol.*, *25*, 1523–1530.

Rao, V. B., C. C. Ferreira, S. H. Franchito, and S. S. V. S. Ramakrishna (2008), In a changing climate weakening tropical easterly jet induces more violent tropical storms over the north Indian Ocean, *Geophys. Res. Lett.*, *35*, L15710, doi:10.1029/2008GL034729.

Reynolds, R. W., N. A. Rayner, T. M. Smith, D. C. Stokes, and W. Wang (2002), An Improved In Situ and Satellite SST Analysis for Climate, *J. Climate*, *15*, 1609–1625.

Rienecker, M. M., et al. (2011), MERRA - NASA's Modern-Era Retrospective Analysis for Research and Applications, *J. Climate*, *24*, 3624–3648, doi:10.1175/JCLI-D-11-00015.1.

Roy, S. S., and N. S. Roy (2011), Influence of Pacific decadal oscillation and El Niño Southern oscillation on the summer monsoon precipitation in Myanmar, *Inter. J. Climatol.*, *31*, 14–21.

Saha, S., et al. (2010), The NCEP Climate Forecast System Reanalysis, *Bull. Amer. Meteor. Soc.*, *91*, 1015–1057.

Sen Roy, N., and S. Kaur (2000), Climatology of monsoon rains of Myanmar (Burma), *Inter. J. Climatol.*, *20*, 913–928.

Simmons, A. S., D. D. Uppala, and S. Kobayashi (2007), ERA-interim: new ECMWF reanalysis products from 1989 onwards, *CMWF Newsl*, *110*, 29–35.

Singh, O. P., T. M. Ali Khan, and M. S. Rahman (2000), Has the frequency of intense tropical cyclones increased in the north Indian Ocean? *Curr. Sci.*, *80*, 575–580.

Smith, T. M., and R. W. Reynolds (2003), Extended Reconstruction of Global Sea Surface Temperatures Based on COADS Data (1854-1997), *J. Climate*, *16*, 1495–1510.

Taylor, K. E., R. J. Stouffer, and G. A. Meehl (2011), An Overview of CMIP5 and the Experiment Design, *Bull. Amer. Meteor. Soc.*, *93*, 485–498.

Uppala, S. M., et al. (2005), The ERA-40 re-analysis, *Q. J. R. Meteorolog. Soc.*, *131*, 2961–3012.

Wang, S.-Y., R. E. Davies, W.-R. Huang, and R. R. Gillies (2011), Pakistan's two-stage monsoon and links with the recent climate change, *J. Geophys. Res.*, *116*(D16), 27, doi:10.1029/2011JD015760.

Wang, B., S. Xu, and L. Wu (2012), Intensified Arabian Sea tropical storms, *Nature*, *489*, 7416.

Webster, P. J. (2008), Myanmar's deadly daffodil, *Nature Geosci.*, *1*, 1752–0894.

Wu, G., Y. Guan, Y. Liu, J. Yan, and J. Mao (2012), Air–sea interaction and formation of the Asian summer monsoon onset vortex over the Bay of Bengal, *Clim. Dynamics*, *38*, 261–279.

Xie, P., and P. A. Arkin (1997), Global Precipitation: A 17-Year Monthly Analysis Based on Gauge Observations, Satellite Estimates, and Numerical Model Outputs, *Bull. Amer. Meteor. Soc.*, *78*, 2539–2558.

Yanase, W., H. Taniguchi, and M. Satoh (2010), The Genesis of Tropical Cyclone Nargis (2008): Environmental Modulation and Numerical Predictability, *J. Meteorol. Soc. Jpn. Ser. II*, *88*, 497–519.

Yatagai, A., K. Kamiguchi, O. Arakawa, A. Hamada, N. Yasutomi, and A. Kitoh (2012), APHRODITE: Constructing a Long-Term Daily Gridded Precipitation Dataset for Asia Based on a Dense Network of Rain Gauges, *Bull. Amer. Meteor. Soc.*, *93*, 1401–1415.

Yokoi, S., and Y. N. Takayabu (2010), Environmental and External Factors in the Genesis of Tropical Cyclone Nargis in April 2008 over the Bay of Bengal, *J. Meteorol. Soc. Jpn. Ser. II*, *88*, 425–435.

Yoon, J.-H., and T.-C. Chen (2005), Water vapor budget of the Indian monsoon depression, *Tellus A*, *57*, 770–782.

Yu, J., and Y. Wang (2009), Response of tropical cyclone potential intensity over the north Indian Ocean to global warming, *Geophys. Res. Lett.*, *36*, L03709, doi:10.1029/2008GL036742.